

Recent advances of interface engineering ininverted perovskite solar cells

Shiqi Yu(余诗琪), Zhuang Xiong(熊壮), Zhenhan Wang(王振涵), Haitao Zhou(周海涛), Fei Ma(马飞),Zihan Qu(瞿子涵), Yang Zhao(赵洋), Xinbo Chu(楚新波), and Jingbi You(游经碧)

Citation: Chin. Phys. B, 2022, 31 (**10**): 107307. DOI: 10.1088/1674-1056/ac8e9f

Journal homepage: http://cpb.iphy.ac.cn; http://iopscience.iop.org/cpb

What follows is a list of articles you may be interested in

Surface modulation of halide perovskite films for efficient and stable solar cells

Qinxuan Dai(戴沁煊), Chao Luo(骆超), Xianjin Wang(王显进), Feng Gao(高峰), Xiaole Jiang(姜晓乐), and Qing Zhao(赵清)

Chin. Phys. B, 2022, 31 (**3**): 037303. DOI: 10.1088/1674-1056/ac1fe0

High-performance self-powered photodetector based on organic/inorganic hybrid van der Waals heterojunction of rubrene/silicon

Yancai Xu(徐彦彩), Rong Zhou(周荣), Qin Yin(尹钦), Jiao Li(李娇), Guoxiang Si(侣国翔), and Hongbin Zhang(张洪宾)

Chin. Phys. B, 2021, 30 (**7**): 077304. DOI: 10.1088/1674-1056/abf345

Band alignment of p-type oxide/ε-Ga_2O_3 heterojunctions investigated by x-ray photoelectron spectroscopy

Chang Rao(饶畅), Zeyuan Fei(费泽元), Weiqu Chen(陈伟驱), Zimin Chen(陈梓敏), Xing Lu(卢星), Gang Wang(王钢), Xinzhong Wang(王新中), Jun Liang(梁军), Yanli Pei(裴艳丽)

Chin. Phys. B, 2020, 29 (**9**): 097303. DOI: 10.1088/1674-1056/ab9c0d

Energy band alignment at Cu_2O/ZnO heterojunctions characterized by *in situ* x-ray photoelectron spectroscopy

Yan Zhao(赵妍), Hong-Bu Yin(尹泓卜), Ya-Jun Fu(符亚军), Xue-Min Wang(王雪敏), Wei-Dong Wu(吴卫东)

Chin. Phys. B, 2019, 28 (**8**): 087301. DOI: 10.1088/1674-1056/28/8/087301

Analysis of displacement damage effects on bipolar transistors irradiated by spallation neutrons

Yan Liu(刘岩), Wei Chen(陈伟), Chaohui He(贺朝会), Chunlei Su(苏春垒), Chenhui Wang(王晨辉), Xiaoming Jin(金晓明), Junlin Li(李俊霖), Yuanyuan Xue(薛院院)

Chin. Phys. B, 2019, 28 (**6**): 067302. DOI: 10.1088/1674-1056/28/6/067302

TOPICAL REVIEW — Celebrating 30 Years of *Chinese Physics B*

Recent advances of interface engineering in inverted perovskite solar cells

Shiqi Yu(余诗琪)[1,2], Zhuang Xiong(熊壮)[1,2], Zhenhan Wang(王振涵)[1,2], Haitao Zhou(周海涛)[1,2], Fei Ma(马飞)[1,2], Zihan Qu(瞿子涵)[1,2], Yang Zhao(赵洋)[1,2], Xinbo Chu(楚新波)[1,2], and Jingbi You(游经碧)[1,2,†]

[1] *Key Laboratory of Semiconductor Materials Science, Institute of Semiconductors, Chinese Academy of Sciences, Beijing* 100083, *China*
[2] *Center of Materials Science and Optoelectronics Engineering, University of Chinese Academy of Sciences, Beijing* 100049, *China*

(Received 2 August 2022; revised manuscript received 28 August 2022; accepted manuscript online 2 September 2022)

Perovskite solar cells (PSCs) have witnessed great achievement in the past decade. Most of previous researches focus on the n–i–p structure of PSCs with ultra-high efficiency. While the n–i–p devices usually used the unstable charge transport layers, such as the hygroscopic doped spiro-OMeTAD, which affect the long-term stability. The inverted device with the p–i–n structure owns better stability when using stable undoped organic molecular or metal oxide materials. There are significant progresses in inverted PSCs, most of them related to charge transport or interface engineering. In this review, we will mainly summarize the inverted PSCs progresses related to the interface engineering. After that, we prospect the future direction on inverted PSCs.

Keywords: inverted perovskite solar cells, charge transport layer, interface modification, defect passivation

PACS: 73.40.Lq, 68.65.–k, 68.35.–p, 81.05.Hd **DOI:** 10.1088/1674-1056/ac8e9f

1. Introduction

Metal halide perovskite materials have attracted extensive attention in the field of solar cells due to the optoelectronic properties such as high absorption coefficient, tunable bandgap, large carrier diffusion length and small exciton binding energy.[1–6] After several years of development,[7–18] since Miyasaka *et al.* first applied perovskite materials into solar cells in 2009,[12] the power conversion efficiency (PCE) of PSCs has rapidly increased from the original 3.8% to the certified 25.7%.[19]

In perovskite solar cells (PSCs) devices, the absorption layer with ABX_3 (A = MA$^+$/methylammonium$^+$, FA$^+$/formamidinium$^+$, generally with the mixture of Cs$^+$ or Rb$^+$; B = Pb^{2+} or Sn^{2+}; X = I$^-$ or Br$^-$) structure[20–23] (Fig. 1(a)) is sandwiched between the n-type electron-transporting layer (ETL) and p-type hole-transporting layer (HTL). Based on the deposition sequence of the charge layers, there are two typical device structures for PSCs: n–i–p type (named as normal structure, Fig. 1(b)) and p–i–n type (named as inverted structure, Fig. 1(c)). In particular, the PSCs with p–i–n structure deserve more attention for further study on account of their long-term stability and negligible hysteresis effects,[24,25] which promise the evolution of PSCs in the commercial market.

Compared to the normal structure of PSCs using moisture/heat-sensitive doped charge transport layer, stable undoped organic semiconductor or metal oxide is usually used in the inverted PSCs, which shows the great advantage in the long-term stability of the inverted PSCs.

It has been mentioned that the p–i–n PSC was first proposed in 2013 by Guo *et al.* based on organic solar cells architecture.[26] The highest efficiency of the inverted PSCs is 25.0% (with certified 24.3%), which is comparable to the champion efficiency of normal structure PSCs.[27] In addition to the development of the perovskite film growth technique, the main driving force for higher performance in inverted perovskite solar cells mainly is due to the interface engineering. In this review, we focus on summary of the recent milestone progresses in inverted PSCs, especially in the interface engineering including the hole transport layer, electron transport layer and their modifications.

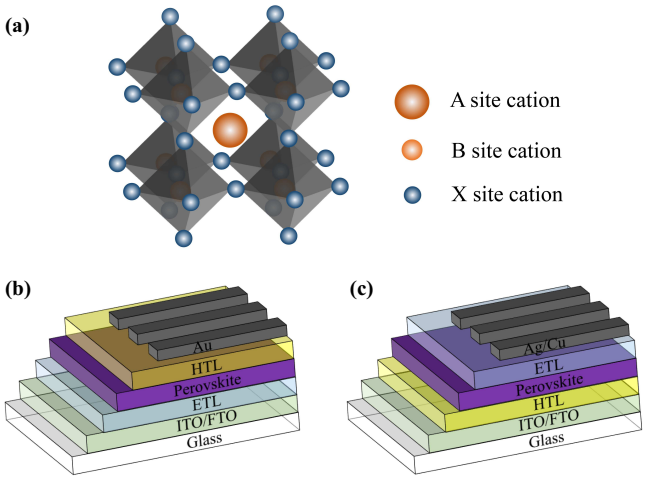


Fig. 1. (a) Schematic diagram of perovskite crystal structure. (b) and (c) Normal and inverted structure perovskite solar cells, respectively.

†Corresponding author. E-mail: jyou@semi.ac.cn

© 2022 Chinese Physical Society and IOP Publishing Ltd

2. Hole transport layers of PSCs

Both organic and inorganic semiconductors are widely used as the HTL in inverted PSCs. Since the HTL is on the bottom of the device, acts as the optically active window, the charge selective layer and the substrate for perovskite at the same time in inverted PSCs, the characters of HTLs dominate both the quality of the resultant perovskite films and the light absorption (performance) of the devices. Hence, it is considered that high transmittance, appropriate energy level and surface properties are required for the HTL in high-perform inverted PSCs. Meanwhile, the contact between HTL and perovskite, that is the buried interface, largely determines the device performance.[28,29] Several mainstream hole transport materials and their interface modification are introduced.

2.1. Organic HTLs for inverted PSCs

2.1.1. PTAA based inverted PSCs

Poly[bis(4-phenyl)(2,5,6-trimethylphenyl)amine] (PTAA) is regarded as a splendid hole transporting and electron blocking material in perovskite solar cells. The molecular structure of PTAA is displayed in Fig. 2(a). In 2014, PTAA was introduced into normal PSCs by replacing classic hole transport layer Spiro-OMeTAD, and an excellent performance of 16.2% was achieved by Gratzel and Seok *et al.*[3] Now, PTAA is used as a general and efficient hole transport layer for inverted perovskite solar cells.

Huang and co-workers firstly introduced the PTAA into the inverted PSCs and they found that the hydrophobic properties of PTAA affect the growth of the perovskite layer. The PTAA showed a great capability to increase the open-circuit voltage (V_{OC}) of PSCs after a post-washing process by DMF. In addition, a short-time ultraviolet (UV) treatment of the PTAA layer before the perovskite deposition changes the hydrophobicity of PTAA surface and improves the optical properties of PTAA layers either. As a result, the UV treatment for doping-free PTAA HTL helped the inverted devices to get a high PCE of 19.17%.[30] When applying 2,3,5,6-tetrafluoro-7,7,8,8-tetracyanoquinodi-methane (F4-TCNQ) doped PTAA as the HTL, a steady-state PCE of 21% at the maximum power point in the F4-TCNQ-doped PTAA based inverted PSCs was achieved by Zhu *et al.* while PTAA was pre-treated by DMF solvent after annealing process.[31] However, F4-TCNQ has poor solubility in toluene, which is a common solvent for PTAA.

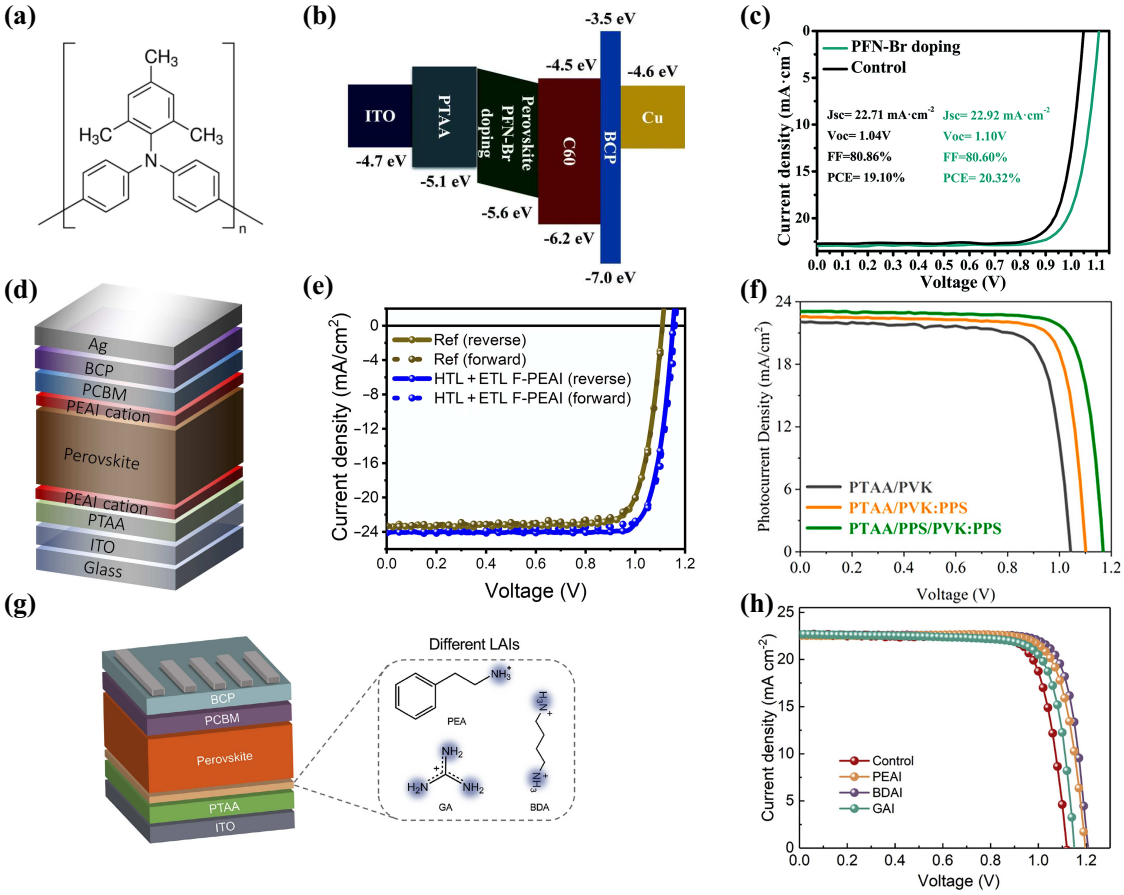


Fig. 2. (a) Molecular structure of PTAA. (b) The energy levels of PFN-Br doped devices and (c) *J*–*V* curves of the champion control device and PFN-Br doped device.[32] (d) Solar cell device structures with the passivated interfaces and (e) *J*–*V* curves of champion reference and FPEAI modified device.[34] (f) *J*–*V* curves of PTAA/PVK, PTAA/PVK:PPS, and PTAA/PPS/PVK:PPS-based devices.[35] (g) Schematic of inverted devices structure and the chemical structure of LAIs and (h) *J*–*V* curves of the control device and devices based on different LAIs.[37]

Researchers found that the wettability of charge transport layers can be improved by introducing an amphiphilic conjugated polyelectrolyte as interfacial compatibilizer. The poly [(9,9-bis(3′-(N,N-dimethylamino)propyl)-2,7-fluorene)-alt-2,7-(9,9dioctylfluorene)] (PFN) or poly [(9,9-bis(30-((N,N-dimethyl)-N-ethylammonium)-propyl)-2,7-fluorene)-alt-2,7-(9,9-dioctylfluorene)] dibromide (PFN-P2) is demonstrated to perfectly change the hydrophobicity of PTAA, thus reducing the interfacial contact losses at both the surface and bottom interface. As the result, a large increase in V_{OC} was realized, and an efficiency of 20.32% was obtained in devices (Figs. 2(b) and 2(c)).[32] Xing's group applied a donor–acceptor–donor type organic molecule, 4,4′,4″-(1-hexyl-1H-dithieno [3′,2′:3,4;2″,3″:5,6] benzo [1,2-d] imidazole-2,5,8-triyl) tris (N,N-bis(4-methoxyphenyl)aniline) (denoted as M2), to modify the surface of PTAA. M2 was designed to be benefit for hole extraction and transport, and finally improved the PCE from 18.67% to 20.23%.[33]

Inserting ultrathin interlayers between perovskite and charge transport layers is a ubiquitous method to substantially reduce these interfacial contact losses at both the up and down interfaces. The incorporation of the 2-phenylethylammonium iodide (PEAI) small molecules in DMF gives rise to an amelioration of the device performance. Except for the modifying effect of DMF in surface wettability, PEAI improves the interface contacts by facilitating high-quality film formation upon the HTL. The modification of the bottom interface leads to a more compact and uniform perovskite film with less nanovoids, resulting in a significant increase in the fill factor (FF) from 83.4% to 85%, thus achieving a superior device performance of 23.7% (Figs. 2(d) and 2(e)).[34] The phenyl group of PEAI can tightly bound to the face-on PTAA polymers due to π-π stacking, thus generating the upward-facing alignment of the ethylammonium iodide group, which is deemed to be the nucleation points for the growth of perovskite crystals. Similarly, a steady chemical bridge is constructed between the interface of 3-(1-pyridinio)-1-propanesulfonate (PPS) molecules and PTAA to lessen interfacial recombination centers for charge carriers. The sulfonate at the other end of PPS could anchor perovskite through a strong S–O•••Pb coordination bond at the same time. Therefore, the charge collection takes advantage of the chemical bridge and the recombination is suppressed on the contrary, leading to an efficiency of 21.7% (Fig. 2(f)).[35]

Huang *et al.* developed a blade-coating technique for the fabrication of PTAA and perovskite thin films in large-area devices at room temperature. Partial substitution of dimethyl sulfoxide (DMSO) with solid-state carbohydrazide minimizes interfacial pinholes and inhibits the crystallization process, resulting in larger grains and intimate contact at HTL/perovskite interface. Thus, the inverted PSCs get a stabilized PCE of 23.6% for single device and an efficiency of 19.2% for module.[36] Although ultra-thin polymers have been confirmed to be successfully in inhibiting non-radiative recombination at the bottom interface, the following problem is that the insulating films may impede the extraction of charge. Alex Jen and co-workers employed a large alkylammonium interlayer (LAI) to improve the interface contact between PTAA/PVSK. 1,4-butanediammonium iodide (BDAI) shows outstanding performances in defects passivation and crystal-growth facilitation simultaneously. Thus they achieved a dramatically increased V_{OC} from 1.12 V to 1.21 V, yielding a PCE of 22.3% (Figs. 2(g) and 2(h)).[37] Usually, there exists a trade-off between the solubility and molecular weight of polymers, so the influence of PTAA polymers' molecular weight on solubility should be considered in inverted PSCs.

2.1.2. P3CT-X HTL based inverted PSCs

Poly[3-(4-carboxybutyl)thiophene-2,5-diyl] (P3CT) molecule acts as an efficient HTM in the p–i–n structure in recent years. The P3CT-based polymers contain the hydrophilic side chains, which are beneficial to the solubility of the material in deionized water. The P3CT-X (X: Na^+, K^+, Rb^+, Cs^+, or $CH_3NH_3^+$) polymer is synthesized via mixing P3CT with other compounds. The molecular structure of P3CT-Na is shown in Fig. 3(a), which is synthesized through the substitution of hydrogen anion by sodium anion in P3CT, when mixing P3CT and NaOH in water solution. Fang *et al.* have rich experience in the synthesis of P3CT-X compounds and have successfully used them in preparing high-efficiency inverted PSCs. At the beginning, moderate efficiency of 16.6% has been obtained, which was mainly attributed to the hydrophilicity of Na^+ ions.[38] The concentration of P3CT-Na aqueous solution is approximately 0.15 wt%, indicating that Na^+ barely changes the solubility of P3CT in water. When the Na^+ is substituted by $CH_3NH_3^+$, they obtained a smoother interlayer film on the substrate. Moreover, P3CT-CH_3NH_2 has better solubility in methanol and shows a stronger aggregation, comparing with P3CT-Na. As a result, the efficiency increased dramatically from 16.6% to 19.6% (Fig. 3(b)). Furthermore, devices based on flexible polyethylene terephthalate (PET) substrate achieved 18.2% (Fig. 3(c)).[39] The doping of graphdiyne (GD) in P3CT-K effectively improves the surface wettability, and subsequently, resulting in better morphology, homogeneous coverage and reduced grain boundaries. Finally, the PCE of P3CT-K based inverted PSCs achieved 19.5% (Figs. 3(d) and 3(e)).[40] Considering the affinity of alkali metal ions Rb^+ and Cs^+ with perovskite materials, researchers investigated the performance of the Rb^+/Cs^+doped P3CT as the HTLs. Figure 3(f) exhibits the energy level diagram of P3CT-X polymers composed of different elements. It is as expected that the work function (WF) of P3CT-Rb matches

well with the valence band of perovskites, generating a large open-circuit voltage and high efficiency of 20.52% (Figs. 3(g) and 3(h)).[41] While introducing PbS buffer layer, combing using the synthetic P3CT-N material as the hole transport layer, an efficiency of up to 24.3% has been achieved, which is the highest level of inverted PSCs at present.[42]

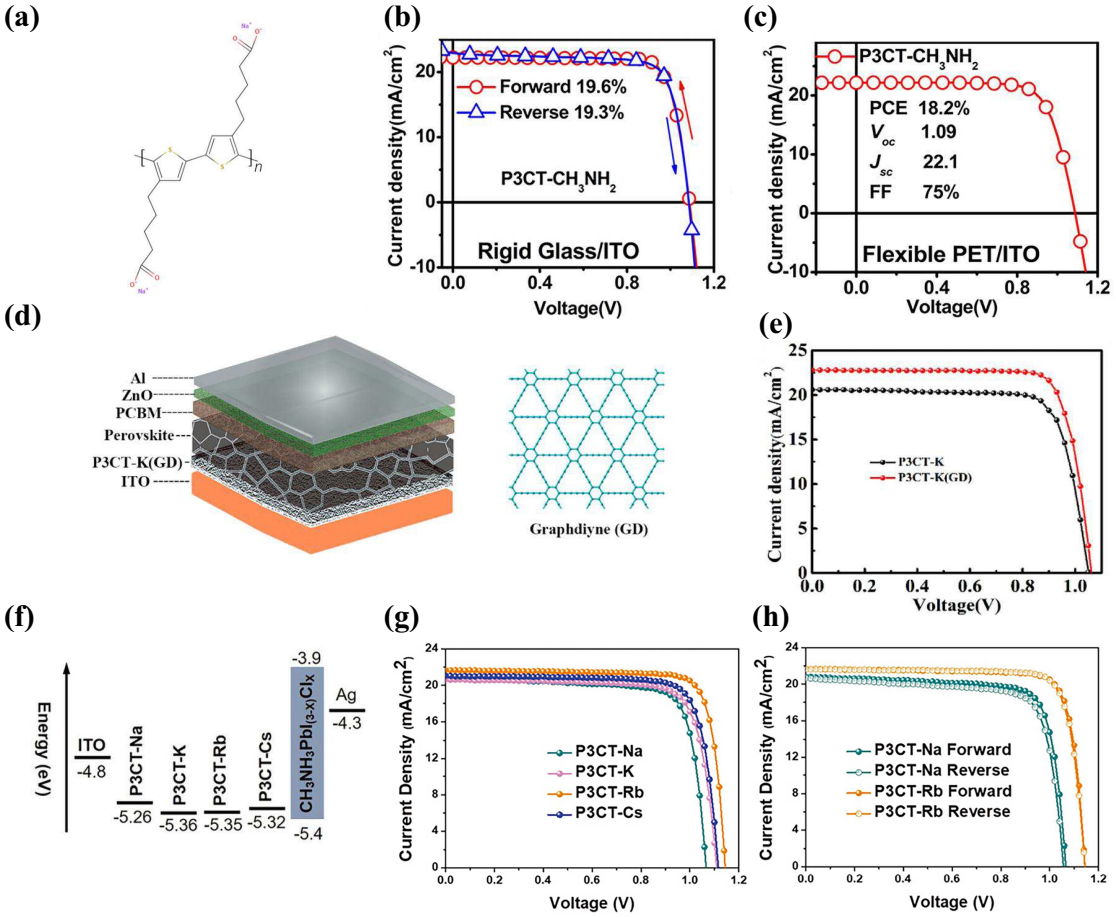


Fig. 3. (a) Molecular structure of P3CT-Na. *J*–*V* curves of devices with P3CT-CH_3NH_2 on (b) rigid glass/ITO and (c) flexible PET/ITO.[39] (d) Device architecture and the structure of GD and (e) *J*–*V* curves of devices with P3CT-K and P3CT-K(GD) as HTLs.[40] (f) Energy level diagram of the P3CT-X polymer; (g) *J*–*V* curves and (h) hysteresis of devices based on different HTLs.[41]

2.1.3. Organic self-assembled molecules based inverted PSCs

Self-assembly means the process by which a disordered system forms an organized structure through the interactions of individual components without external intervention. Figure 4(a) shows the basic structure of a self-assembled molecule (SAM) which includes three portions: the anchoring, the spacer and the terminal groups.[43] The anchoring groups of SAMs can form covalent links to the substrate, which guarantees high coverage of the SAM. For example, the aliphatic phosphonic acids [—P(=O)$(OH)_2$] can easily compose a dense insulating monolayer on oxides and block the electron transfer across the interface.[44,45] The spacer group is the backbone of the molecule, it bridges terminal and anchoring groups. The terminal group is in charge of the interfacial chemistry with the overlayer (e.g., the energy level alignment) and determining surface properties (e.g., the hydrophily).

After previous application as electrode modifications, SAM was first used as the hole-selective layer on ITO for inverted PSCs in 2018 and got a PCE of 17.8%.[44] Up to now, the single junction inverted devices own the efficiency of 24.3%[46] and the tandem devices of 29.1%[47] as the best level. Different from conventional organic HTLs which are usually costly and doping-required, SAMs present multiple advantages, including simple synthesis methods, tunable bandgap and green-solvent inclusiveness. For instance, except for conventional spin-coating, the dip-coating method is especially suitable for large-area and textured substrates. With the immersion and rinsing progress, the substrate obtained by dip-coating is comparable to the spin-coating one. Various self-assembled molecules with different structures can be designed and synthesized according to different requirements. The SAMs are designed to modulate the work function to align with the valence band of perovskite. Phosphonic acids (PA) are widely known to form strong links with oxide surfaces and enable work function modulation. In addition, carbazole derivatives have been demonstrated for their electron-blocking and hole-selective properties. SAMs

based on carbazole show great superiority in defects passivation and charge extraction optimization. Figure 4(b) exhibits the molecule structures of several carbazole-based SAMs, e.g., V1036 ((2-{3,6-bis[bis(4-methoxyphenyl)amino]-9H-carbazol-9-yl}ethyl)phosphonic acid),[44] MeO-2PACz ([2-(3,6-dimethoxy-9Hcarbazol-9-yl)ethyl]phosphonic acid) and 2PACz ([2-(9H-carbazol-9-yl)ethyl]phosphonic acid). The performances of devices based on such SAMs are presented in Figs. 4(c) and 4(d).[48] Based on 2PACz, the efficiency of the inverted devices gradually increased from 21.1% up to 24.3%, which is the most outstanding performance at present.[46,49] Studies show that the passivation effect and charge extraction ability of SAMs are greatly improved after replacing methoxyl group with methyl group in MeO-2PACz. Meanwhile, the impact of the aliphatic chain length (n) in carbazole-based SAMs was explored and the results reveal a maximal FF at $n = 2$ for nPACz and $n = 4$ for Me-nPACz.[47,50] Therefore, a FF of 84% in inverted PSCs was achieved with the Me-4PACz HTL (Fig. 4(e)). Besides, the high efficiency of 29.1% could be achieved when it is applied in the perovskite/silicon tandem solar cells,[47] as displayed in Figs. 4(f) and 4(g).

Additionally, small molecule materials with different structures are also competitive, such as EDAR03, MPA-BT, Br-2EPT, with superior ability of charge collection and enable highly stable and efficient devices with PCE of around 22% (Figs. 4(h) and 4(i)).[51–53] SAMs can act as a buffer between HTL/perovskite as well. To align the energy level of each layer in devices, SAMs were used to modify hole transport layers. This will be discussed in the next sections.

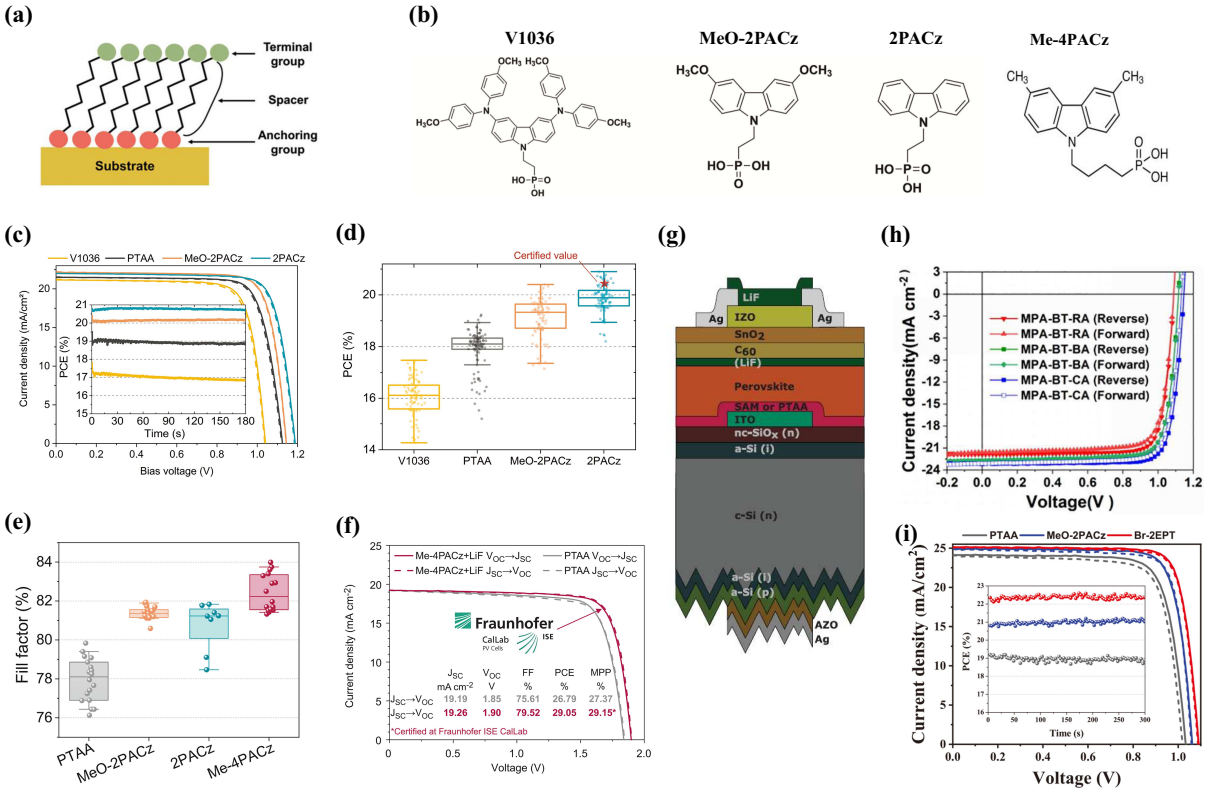


Fig. 4. (a) Schematic diagrams of three constituent parts in SAM.[43] (b) Chemical structure diagrams of several SAMs. (c) J–V curves of SAM-based devices in comparison to state-of-the-art PTAA devices with respective MPP tracks in the inset and (d) box plot of PCE values for devices based on different HTLs.[48] (e) Comparison of fill factor values of p–i–n devices with different hole-selective layers; (f) certified J–V curves using various HTLs and (g) schematic stack of perovskite/silicon tandem solar cells.[47] (h) J–V curves of the best-performing devices based on the various MPA-BT-X SAMs.[52] (i) J–V curves of the best-performing devices based on PTAA and SAMs with respective MPP tracks in the inset.[53]

2.2. Inorganic nickel oxide for inverted PSCs

NiO_X is widely used as the p-type HTL in dye-sensitized solar cells (DSSCs) and organic photovoltaics (OPV), thus it is a good alternative for PSCs.[54,55] In inverted PSCs, NiO_X is a promising inorganic hole transport material (HTM) for its wide bandgap (3.6 eV), deep valence band (5.2–5.4 eV), and high carrier mobility (0.1 cm^2/Vs).[56] Several methods have been reported for the fabrication of NiO_X HTL, such as atomic layer deposition (ALD), magnetron sputtering, sol-gel, metal–organic chemical vapor deposition, spray pyrolysis, and molecular beam epitaxy.[57] In particular, the solution processes are feasible at low temperatures. NiO_X shows p-type characteristics due to the existence of nickel vacancies and the considerable ionization energy of the Ni vacancies leads to the low intrinsic conductivity. Another issue is that the Fermi level of NiO_X is still far from the valence band edge of the perovskite, which brings a large energy level shift at the interface between NiO_X and the perovskite layer. Various methods have been developed to optimize the conductivity or work function

of NiO_X, mainly divided into three routes: UV/oxygen plasma treatment, surface modification and extrinsic additive.

NiO_X performed poorly (PCE $\approx 0.1\%$) as the hole transport layer in the first time, owing to the poor coverage of perovskite on NiO_X surface. The connection between HTL/ETL may result in short circuit in devices.[58] With the improvement of the preparation process and materials, NiO_X can cover the substrate surface uniformly and improve the crystal quality of the perovskite film, yielding higher efficiency in NiO_X based PSCs than PTAA. Oxygen plasma treatment for the NiO_X film significantly affects the wettability and electrical conductivity, especially in the work function. As a result, the recombination rate at the interface of NiO_X/perovskite is increased and the grain size of perovskite becomes larger. The influence of NiO_X thin films gradually improved as the exposure duration increased. With an optimal exposure time of five minutes, an efficiency of 19.67% was achieved.[59] By the ALD technology, dense and extremely thin HTL of NiO_X can be obtained without any pinholes. In this way, the film thickness is under precise control and the interface alignment between NiO_X and perovskite can be adjusted to match the charge transport with comparable conductivity. It has been reported by Seo *et al.* that an apparent increase in the work function of ultrathin NiO_X can be observed when the thickness is comparable to its Debye length.[60] Furthermore, an annealing treatment of NiO_X thin film is beneficial to the reduction of hydroxylated NiOOH and C-H defects, resulting in better interfacial properties.[61]

Nevertheless, studies have shown that effective modification of the NiO_X/perovskite interface remains a key challenge in achieving high V_{OC} values for NiO_X based inverted PSCs, whereas high V_{OC} lost is usually attributed to the surface defects of NiO_X arising from the low-temperature process. Thus, surface modification rises in response to the conditions. Yang's group suggested a surface modification strategy to alter the quality of NiO_X. With the treatment of diethanolamine (DEA), it provides extra chemical bonding between the NiO_X and perovskite layer which improves the quality of the perovskite film and increase the device performance close to 16% PCE with a rather high FF.[62] Moreover, as self-assembled monolayers coming into people's sight, Alex *et al.* compared a series of self-assembled molecules with different terminal groups and found that the gas-phase dipole moments of benzoic acid derivatives varied greatly, among which Br-BA presents the strongest dipolar interactions. Hence, the Br-BA modified devices presented better stability and enhanced PCE from 15.5% to 18.4%, and an efficiency of 16.2% was achieved on PET substrate.[63] NiO_X film can provide a feasible contact for the homogeneous growth of SAM, compared to the direct contact with ITO. There is an increase in shunt resistance with the combination of NiO_X and MeO-2PACz, leading to a harvest of more than 50 mV in V_{OC} and FF of 7%, absolutely. The uniform MeO-2PACz layer on NiO_X leads to better repeatability of device after comparison in batches of devices, as shown in Fig. 5(a), and the enhanced interface contact enables the device with 20% PCE.[64] Similarly, organic small molecules and polymers are used for surface modification of NiO_X either. Park *et al.* designed a serious group of Lewis-based organic molecules as the interface layer between NiO_X and perovskite layer, which can work as HTLs and surface modifiers simultaneously.[65] The effects of polymers, such as PTAA, polystyrene (PS), and poly(methyl methacrylate) (PMMA), on the NiO_X based inverted devices were investigated. It was reported that all these three polymers are in favor of smoother surface and less defect states. However, PMMA provides additional assistance in defect passivation because of the interaction between its carbonyl and methoxy group with Pb^{2+}, increasing the V_{OC} up to 1.19 V in the modified devices. Moreover, PTAA provides a better energy level alignment by deepening the HOMO level of bare NiO_X, which matches well with the perovskite and thereby reduces the interface energy loss. As shown in Figs. 5(b) and 5(c), the NiO_X/PTAA based device exhibits the best performance of 21.56%.[66] On the basis of the NiO_X/PTAA architecture, a mesoporous alumina layer can be inserted to obtain devices with higher efficiency of 21.9% (Figs. 5(d)–5(f)).[67] The wide-band-gap mp-Al_2O_3 layer acts as not only a scaffold but also an electron-blocking layer, and the compact ALD-SnO_2 top layer in devices gives a great favor to the stability, which remains above 85% after 1000 hours under continuous illumination.

Researchers discovered that doping or alloying NiO_X with metal elements can greatly raise the conductivity of the HTL. Generally, metal ions are added during the preparation of NiO_X. Copper (Cu^{2+}) is one of the most popular dopant elements of NiO_X since Cu^{2+} can easily occupy the Ni sites with the similar ion radius. Copper-doped NiO_X (Cu:NiO_X) resulted in a device PCE of 17.8% under low-temperature process at first.[68] Subsequently, researchers developed a bi-layer structure of Cu:NiO_X to minimize the recombination loss at the NiO_X/perovskite interface and achieve a PCE of 19.79%.[69] The Cu:NiO_X HTL with various doping concentrations can be achieved by a high-temperature solid-state reaction under pulsed laser deposition (PLD). 3% Cu:NiO_X films were selected to be the HTL and the resulting device gained the best PCE of 20.41% (Fig. 5(g)).[70] The alkali chloride interface modification of NiO_X HTLs helps to order the crystallization of perovskite layer and reduce trap density (Fig. 5(h)), resulting in a significant improvement in V_{OC} from 1.07 V to 1.15 V. As displayed in Fig. 5(i), potassium chloride preforms best in devices with the PCE approaching 21%.[71] Other similar metal elements (Li, Mg, Co, Cs, Ag, etc.) can also play a positive role in doped-NiO_X by reducing the interfacial resistance at the HTL/perovskite interface.

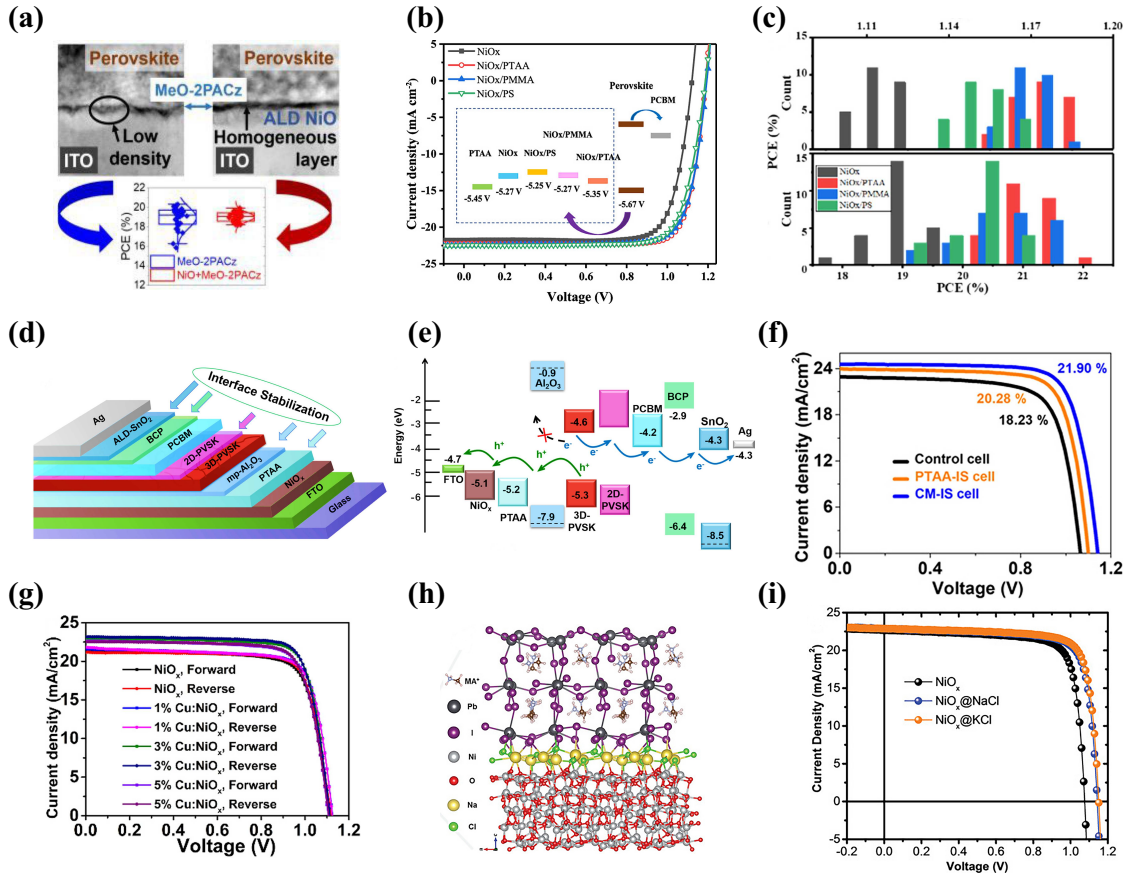


Fig. 5. (a) SEM cross-section and box chart of PCE parameters of devices based on ALD-NiO_X/MeO-2PACz and MeO-2PACz.[64] (b) Energy level alignment and devices characteristics and (c) distribution of V_{OC} and PCE of different polymers modified NiO_X film.[66] (d) Schematic illustration of interface stabilization with effective interfacial layers and (e) corresponding energy band diagram; (f) *J*–*V* curves of devices with or without interlayers.[67] (g) Device characteristics for PSCs with Cu:NiO_X HTLs with different doping concentrations.[70] (h) A supercell illustrating the structural details in perovskite/NaCl/NiO_X HTL interface and (i) *J*–*V* curves of the optimal CsFAMA PSCs with pristine or alkali chlorides modified NiO_X HTLs.[71]

3. Electron transport layers of PSCs

As the counterpart of hole transport layer, electron transport layer plays a crucial role in inverted PSCs for extracting photogenerated electrons and carrier transporting from perovskite to electrodes. Recently, both organic and inorganic electron transport materials are widely studied, such as fullerene and their derivatives or metal oxides. Besides, modifying the interface between ETL/perovskite and perfecting the contact between ETL/electrode are also vital to the efficiency and stability of devices.

3.1. Organic ETLs for inverted PSCs

Fullerene (C_{60}, C_{70}) and their derivatives are widely used as ETLs in inverted PSCs. Phenyl-C61-butyric acid methyl ester (PCBM) is a most used electron acceptor (Lewis acid) by solution process, and it is confirmed that PCBM is an excellent ETL due to its fast electron extraction process between perovskite and PCBM. Sargent *et al.* have demonstrated that the ion migration is significantly suppressed by interacting with uncoordinated halide or Pb-I anti-site defect PbI^{3-}.[72] Li *et al.* also found that PCBM can limit halide-ion migration by halide-π noncovalent interaction.[73] Considering the hysteresis phenomenon of devices, although the cause of hysteresis is still controversial at present (mainly focus on ion migration, ferroelectricity of perovskite and charge traps), there is no doubt that PCBM can effectively restrain hysteresis of solar cells by passivating trap states. In addition, annealing treatment of PCBM increases the short circuit current density (J_{SC}) and FF of devices by enhancing the diffusion of PCBM to the grain boundaries of the perovskite layer.[74] Moreover, researchers combined PCBM and C_{60} to take advantage of the high mobility of C_{60} and get a more proper energy level alignment, for the lowest unoccupied molecular orbital (LUMO) of PCBM is −3.9 eV to −4.2 eV and C_{60} is −4.5 eV.

The surface morphology of PCBM depends on the roughness of the upper surface of the perovskite layer. The discontinuous PCBM film induced by the rough perovskite film results in the poor contact between perovskite and metal electrodes, thus worsening device efficiency and stability. To address this issue, C_{60} is usually evaporated on the surface of PCBM by the thermal evaporation method to form a dense transport layer and barrier layer. In addition, BCP and LiF

have been employed as the hole blocking layer in inverted PSCs by decreasing the effect of electron tunneling.[75] With the structure of PVSK/PCBM/C_{60}/BCP, the efficiency raises up to 20.07% from 17.23%.[76]

N-type doping of PCBM shows better conductivity and electron mobility, yielding better stability in devices. With the dopant of ammonium salt and phosphonium salt, researchers observed that the ionic bonding strength between anion and cation of n-type dopant is critical for electron transport.[77] Employing conjugated n-type polymeric materials as n-dopant in PCBM can form a suitable energy level and guarantee the efficiency exceeding 20.6%. Moreover the high hydrophobicity of the doped ETL is beneficial to the long-term stability of devices.[78] However, the low solubility of PCBM in aromatic solvents is the most critical factor limiting its development, especially for the thickness control of PCBM thin films. Moreover, due to the weak intermolecular interactions in PCBM, the self-aggregation occurs under continuous illumination or heating, which will lead to poor long-term performance of the devices.[79] Structural modification of fullerene is capable to skip this problem. As a result, Li *et al.* synthesized a simple structure of the fullerene derivative with Lewis bases thiophene and amino moieties, named [6,6]-phenyl-C61-butyric acid-N,N-dimethyl-3-(2-thienyl)propanam ester (PCBB-S-N), and the chemical structure is shown in Fig. 6(a). It has been demonstrated that the sulfur atom of thiophene can tightly bond with the uncoordinated Pb^{2+} ions in the perovskite layer, and the amino moiety could form hydrogen bonds to neutralize the migrating iodide ions. As a consequence, the PCE of inverted PSCs achieved 21.08% by constructing a bilayer ETL of PCBB-S-N/PCBM (Fig. 6(b)). It is noteworthy that the stability of the unencapsulated devices has been greatly improved under the ambient atmosphere or heating at 85 °C, which retained almost 95% of its initial efficiencies.[80] Recently, a series of fullerene dyads (F-Cn, $n = 4$, 8, 12) were designed and applied as the ETL in inverted PSCs, as exhibited in Fig. 6(c). Fullerene and terpyridine are connected with different lengths of alkyl chains. It has been proved that the alkyl flexible chain can improve solubility, film-forming ability of ETL, and the terpyridine can chelate with metal cations and suppress fullerene self-aggregation, reducing energy disorder in perovskite. Thus, the devices exhibit a champion PCE of 23.08% when the chain length is $n = 8$. Similarly, the FP-C8/C_{60} based device maintained 96% of the initial PCE after running for 1200 h, the structure and results are shown in Figs. 6(d)–6(g).[81] However, owing to the complex synthesis methods and high costs, it is not widely promoted nowadays for structural modification in organic ETL materials.

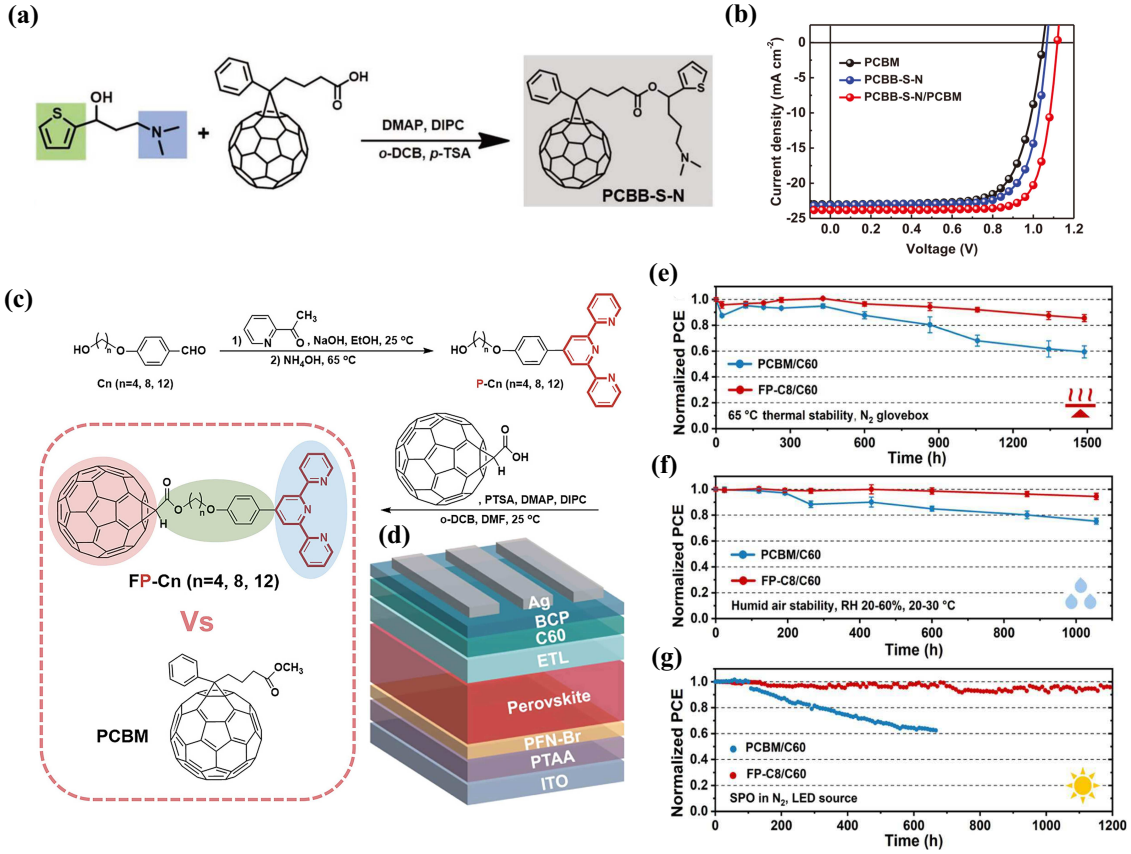


Fig. 6. (a) Synthetic route and chemical structure of PCBB-S-N and (b) *J*–*V* curves of devices with different ETLs (PCBM, PCBB-S-N, PCBB-S-N/PCBM).[80] (c) Synthetic route of FP-Cn ($n = 4$, 8, 12) and chemical structure of PCBM, (d) device structure of the p–i–n planar and (e)–(g) stability of the devices under various conditions.[81]

3.2. Metal oxides as ETLs for inverted PSCs

Inorganic ETMs have superior chemical stability but inferior conductivity when compared with organic ETMs, e.g., ZnO, TiO_2 and SnO_2. However, the energy level mismatch makes it a challenge to achieve state-of-the-art inverted devices with inorganic ETLs alone. Therefore, researchers developed the structure of fullerene/inorganic metal oxide bilayer electron transport layer for obtaining efficient and stable inverted solar cells. With the device architecture of NiO:BN/perovskite/PCBM/ZnO, an improved PCE of 20.74% was achieved.[82] The ZnO nanoparticles are prepared by spin-coating method, which can simply introduce the metal dopant. However, its corrosivity restricts its further improvements. Similarly, niobium (Nb)-doped TiO_2 instead of ZnO enables higher electron mobility and increases the PCE from 18.7% up to 20.7%.[83] A composite consisting of 1D cation-doped TiO_2 brookite nanorod (NR) inlaid by 0D fullerene was applied in inverted PSCs as the top ETL, this 0D:1D composite opens a new dimension for nanomaterials in the application of ETL in PSCs and results in an efficiency exceeding 22%.[84] Recently, atomic layer deposition (ALD) of SnO_2 has been confirmed as the efficient strategy for efficient and stable inverted solar cells. SnO_2 layers grown by ALD at low temperature are optically transparent and electrically conductive, the ultrathin film resists the diffusion of water and oxygen as well as the metal electrode into the perovskite.[85] The device encapsulated by ALD-SnO_2 achieved 23.91% PCE in single-junction devices.[86] The properties of ALD-SnO_2 film make it extremely suitable for tandem perovskite devices. Tan *et al.* have successfully acquired narrow-band gap single-junction PSCs with over 22% PCE and all-perovskite tandem devices with a certified efficiency of 26.4% by atomic layer deposition.[87] Huang *et al.* have also caught up with the step for achieving PCE of 24.4% in all-perovskite tandem solar cells by forming a complex interconnection layer structure of C_{60}/ALD-SnO_2.[88] The perovskite/silicon tandem solar cells with the PCE of over 29%, which have been mentioned above, also adopted the C_{60}/ALD-SnO_2 bilayer and the ALD-SnO_2 served as both hole transport layer and buffer layer.[47] This indicates that inorganic, especially SnO_2, electron transport layer has great potential for future commercial development which requires both high efficiency and high stability.

4. Interface modification of perovskites

In addition to the transport layers, defects and ion migration located at the grain boundaries, surfaces and interfaces are the main factors that limit the device performance as well. The non-radiative recombination originating from these defects results in degradation of materials and devices. Since bulk doping would potentially affect the crystallization of perovskite, interface modification is treated as a convenient method to tackle these problems. The modification of the interface between the perovskite layer and the charge transport layers has been mentioned above partially, aimed at improving the crystallinity of the perovskite and preventing perovskite from degradation generated by moisture and oxygen. Meanwhile, modification inside the perovskite is also required.

Investigations of passivation by incorporation of ionic liquids (ILs) into perovskite ink as well as surface modification were carried out in recent years. ILs are suitable for application in PSCs for their versatile properties, such as high ionic conductivity, thermal and electrochemical stability. The organic ionic solid additive named 1-butyl-1-methylpiperidinium tetrafluoroborate ([BMP][BF_4]) is a compound with a chemically stable organic cation and a [BF_4] anion (Fig. 7(a)). A slight amount of this ionic liquid can effectively reduce the number of available sites for iodide oxidation, thus restrain phase segregation and lead to a steady-state power output of 20.1% (Fig. 7(b)) with the perovskite composition of $Cs_{0.17}FA_{0.83}Pb(I_{0.77}Br_{0.23})_3$.[89] When 1-butyl-3-methylimidazolium tetrafluoroborate ([BMIM][BF_4]) was added to the perovskite precursor, the efficiency increased from 18.5% to 19.8% with enhanced texturing and crystallinity (Fig. 7(c)). ToF-SIMS results revealed that the [BF_4] anion existed mostly at the buried interface while the [BMIM] cation could be probed throughout the bulk film (Figs. 7(d) and 7(e)).[90] It is believed that the ILs additives with similar chemical structure have the same pattern of manifestation in perovskite films. Another pyridinium salt with [BF_4] anion called N-cyanogen-4-dimethylamino-pyridine tetrafluoroborate ([NDAP][BF_4]) was applied as the additive to improve the film quality of perovskite layer. As shown in many studies, the BF_4^- anion is in favor of the grain growth in perovskite, and meanwhile, the pyridine cation has the function of passivating uncoordinated Pb^{2+}. The MA-free inverted PSCs treated by [NDAP][BF_4] promised the efficiency of 21.25% (Fig. 7(f)).[91] With regard to the poly(ionic liquid) (PIL), an imidazolium-based poly-ionic liquid [PeIm][TFSI] was designed to act as multi-functional interlayer in both normal and inverted PSCs. There are similarities between [TFSI] and [BF_4] anion like stabilizing uncoordinated Pb atoms at the upper surface of perovskite. Moreover, the interfacial recombination at the perovskite/ETL interface is strongly suppressed. The champion device got a PCE of 21.4%, and displayed enhanced stability during maximum power point (MPP) tracking under N_2 atmosphere (Figs. 7(g)–7(i)).[92]

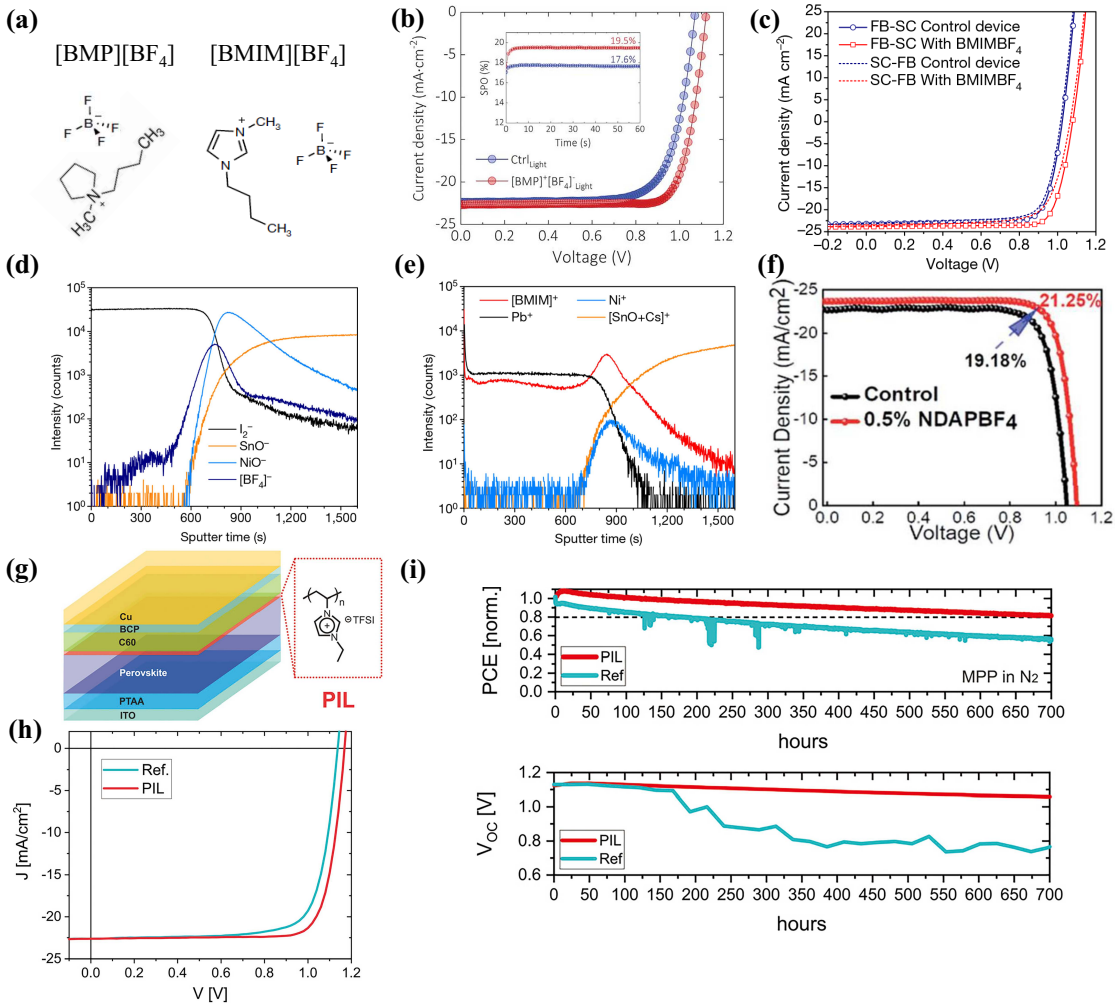


Fig. 7. (a) Chemical structure of $[BMP][BF_4]$ and $[BMIM][BF_4]$. (b) *J*–*V* curves of the $[BMP][BF_4]$ modified and control devices and corresponding steady-state power output.[89] (c) *J*–*V* curves of the best performing device for each condition measured with forward and backward scan, ToF-SIMS depth profiles of the $[BMIM][BF_4]$-containing perovskite film on an NiO/FTO substrate, measured in (d) negative and (e) positive polarity.[90] (f) *J*–*V* curves of the $[NDAP][BF_4]$ modified and control devices and the device structure in inset.[91] (g) Device layer architecture with the chemical structure of the PIL, (h) *J*–*V* curves for a reference untreated device and PIL-modified device, (i) MPP tracking for devices with and without PIL under N_2 atmosphere.[92]

Sorts of cyclobenzene-based molecules and polymers are intensively studied to passivate the surface defects of perovskite, since the superior compatibility with fullerene derivatives that are commonly used as ETL in inverted PSCs. Among all the alkylammonium halogen with benzene, the passivation effect of phenethylammonium (PEA) is the most attractive for the hydrophobic conjugated rings and the electrostatic interactions between PEA^+ and A-site vacancies. Huang *et al.* investigated the passivation effects of diverse molecular functional groups, including carboxyl, amine, isopropyl, phenethyl, and tert-butylphenethyl groups, and they discovered a new type of amino acid passivation molecule, named D-4-tert-butylphenylalanine (D4TBP), which combines all effective passivation groups. The passivation effect of D4TBP is similar to that of PEA, but shows a better efficiency of 21.4% in device.[93] By incorporating a small amount of phenylethylammonium chloride (PEACl) into perovskite inks, crystal growth was facilitated, phase stability was enhanced, ionic defects at the surface and grain boundaries were passivated, thus obtaining a high efficiency of 22.0% with V_{OC} of 1.18 V for blade-coated inverted PSCs.[94] Alex *et al.* reported a rationally designed bifunctional molecule, piperazinium iodide (PI), which acted as not only an electron donor but also an electron acceptor to take reaction with different terminal ends on perovskite surface. PI contains both R_2NH and $R_2NH_2^+$ groups which could form a PbN bond in the single crystal of $(PI)_2PbI_2{\cdot}2DMSO$ as well as the PDI and $(PDI)_2PbI_2$. Obviously, it can passivate uncoordinated Pb^{2+} defects, decrease nonradiative recombination loss and present a more n-type property of perovskite surface for adequate energy transfer. Therefore, a high PCE of 23.37% (with 22.75% certified) could be achieved.[95] Upon the surface treatment of benzenebutanammonium iodide (PBAI), researchers observed the formation of an n–n isotype heterojunction up on the perovskite surface. The local electric field distribution was optimized and ion diffusion was confined, yielding an improve-

ment in the device performance from 20.72% to 23.33% with negligible hysteresis.[96] The dual interfacial modification of 4-fluorophenylethylammonium iodide (F-PAEI) made a huge contribution to the efficiency up to 23.7%, by adding F-PEAI in the antisolvent during the extraction process.[34] Ning *et al.* demonstrated that slight modifications in ligand of PEAI induce preferential growth of quasi-two-dimensional (quasi-2D) ($n \geq 3$) perovskite. With the post-treatment by 3F-PEAI and MAI, 2D and quasi-2D structures were observed on the upper surface of perovskite (Figs. 8(a) and 8(b)). It is verified that quasi-2D treatment can reduce the electron barrier between the 3D and 2D perovskite species to achieve an improved efficiency (certified PCE of 23.9%), as shown in Fig. 8(c).[86] Lately, oleylammonium iodide (OLAI) molecules have been used to passivate trap states and suppress ion migration by forming Ruddlesden–Popper phase 2D perovskite layer. When the post-treatment of OLAI was performed at room temperature, Wolf *et al.* have achieved a PCE of more than 24% with prolonged stability, which tested for over 1200 hours at 85 °C and 85% relative humidity (Figs. 8(d) and 8(e)).[46] Zhu *et al.* have reported a more n-type surface of perovskite film through a solution-processed secondary growth (SSG) technique with guanidinium bromide (GABr), leading to a substantial increase in V_{OC} of 1.21 V without sacrificing electric current. The voltage loss of device is only 0.41 V and the stabilized power output approached 21% at the maximum power point.[31] Another viewpoint is that perovskite can be modified by the n-type and stable inorganic nature of PbS to suppress Pb-rich on the upper surface. The S^{2-} anions would strongly bond with Pb^{2+} at the perovskite interface to complete the process of surface sulfidation. Moreover, the Pb–S bonds induced an extra back-surface field for electron extraction and resulted in a significant improvement in efficiency from 21.8% to 24.3% (Fig. 8(f)).[33] However, the surface modification of alkylammonium salt may induce negative effects in PSCs, such as the unwanted work function shift.[97] By introducing an organometallic compound called ferrocenyl-bis-thiophene-2-carboxylate ($FcTc_2$), Zhu *et al.* successfully functionalized the surface of perovskite films. On one hand, $FcTc_2$ effectively passivated the uncoordinated lead ions with the assistance of the O atom, which could form a strong chemical Pb–O bond. On the other hand, the electron-rich and electron-delocalized ferrocene groups of $FcTc_2$ greatly accelerated the interfacial electron transfer. Thus, the efficiency reached a record level of 25.0% (with certified 24.3%), which is the highest PCE currently known for inverted PSCs (Fig. 8(g)). Moreover, the additional bonding upon perovskite films played a role in the enhancement of stability under various conditions. The encapsulated $FcTc_2$-based devices retained 98% of their original efficiency after 1500 hours under continuous illumination and successfully passed the qualification test of IEC61215:2016 (Figs. 8(h)and 8(i)).[27] Till now, the researchers mainly adopt "25 °C, encapsulated or inert gas protected device, MPP tracing, AM 1.5 light soaking" as the standard test conditions and "85 °C/85% relative humidity" as the accelerated aging test conditions. It is a huge advancement for PSCs to meet the industrial standards like IEC61215:2016.

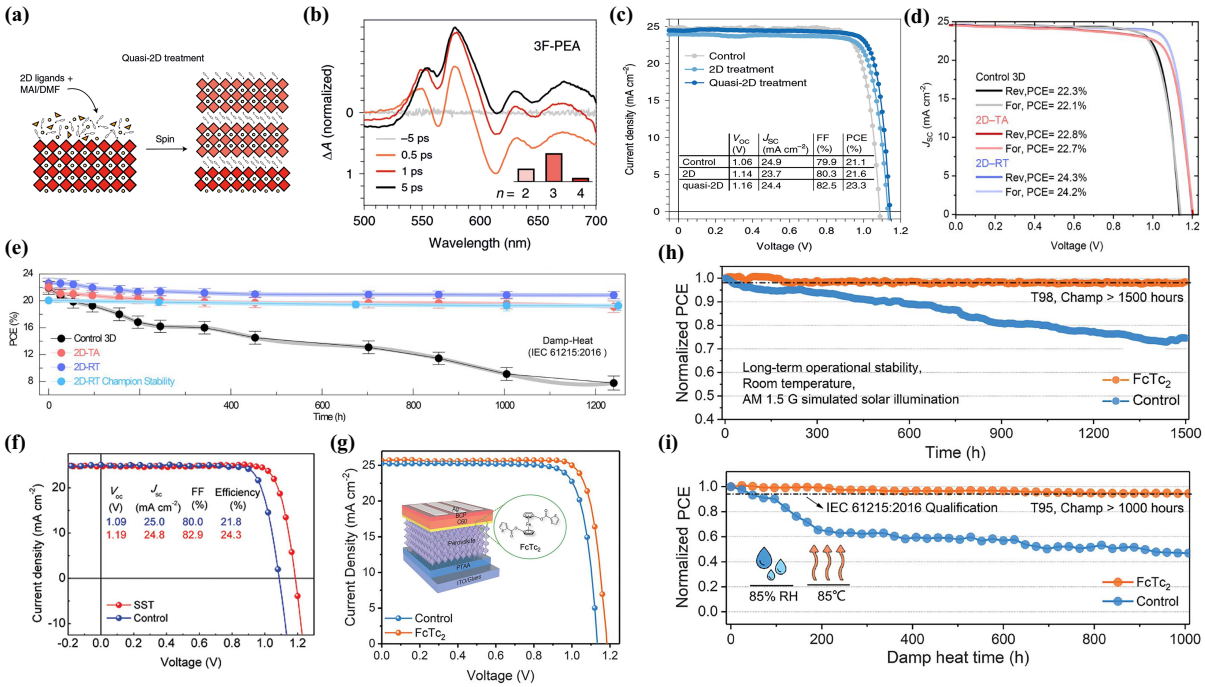


Fig. 8. (a) Schematics of the standard quasi-2D treatment producing $n \geq 2$ reduced-dimensional perovskites, (b) transient absorption spectra of films treated with 3F-PEA and (c) *J*–*V* curves of control, 2D- and quasi-2D-treated devices.[86] (d) *J*–*V* curves and (e) stability of 2D/3D perovskite heterojunction with various treatment.[46] (f) *J*–*V* curves of control and surface sulfidation treatment-based devices.[33] (g) *J*–*V* curves and (h), (i) stability of the champion devices with and without $FcTc_2$.[27]

5. Conclusion and perspectives

After decades of development, the power conversion efficiency of perovskite solar cells (certified PCE of 25.7% for normal structure and reported 25.0% for inverted structure) is gradually approaching crystalline silicon solar cells, which keeps 26.7% for years. The inverted structure has greater advantages in both the preparation process and long-term stability, which accelerates the progress of their commercialization. In order to obtain efficient and stable inverted devices, we review the recent progress of interfacial engineering for both HTL/perovskite and perovskite/ETL interfaces and summarize the modification strategies widely used at present. For the charge transport layers, high conductivity, charge selectivity and hole/electron blocking ability are required. SAMs with roughly similar chemical structures could be the popular selection of the hole transport layer, because they can provide well-matched energy band alignment with different components of perovskite materials. And the common electron transport layers are the bilayer structure of organic materials or metal oxides, which promise the superiority in both efficiency and stability. Regarding to the modification, not only the intrinsic defects of perovskite are noteworthy, but also the interfacial defects need to be handled urgently. Various ammonium and guanidinium halogens are popular materials for the interface treatment at present. The component of perovskite should be taken into account when choosing the modifiers. Currently, the main goal of inverted PSCs remains in improving the efficiency up to par with that of normal devices, since the chemical properties of the materials applied in p–i–n structure are more stable. Additionally, tandem solar cells based on inverted structure are considered as the most promising product to fully take advantage of solar energy in the future.

Acknowledgments

This work was supported by the National Natural Science Foundation of China (Grant No. 61925405) and the National Key Research and Development Program of China (Grant No. 2020YFB1506400).

References

[1] Burschka J, Pellet N, Moon S J, Humphry-Baker R, Gao P, Nazeeruddin M K and Grätzel M 2013 *Nature* **499** 316
[2] Dong Q, Fang Y, Shao Y, Mulligan P, Qiu J, Cao L and Huang J 2015 *Science* **347** 967
[3] Jeon N J, Noh J H, Kim Y C, Yang W S, Ryu S and Seok S I 2014 *Nat. Mater.* **13** 897
[4] Liu M, Johnston M B and Snaith H J 2013 *Nature* **501** 395
[5] Mcmeekin D P, Sadoughi G, Rehman W, Eperon G E, Saliba M, Hörantner M T, Haghighirad A, Sakai N, Korte L, Rech B, Johnston M B, Herz L M and Snaith H J 2016 *Science* **351** 151
[6] Meng L, You J, Guo T F and Yang Y 2016 *Accounts of Chemical Research* **49** 155
[7] Abdi-Jalebi M, Andaji-Garmaroudi Z, Cacovich S, Stavrakas C, Philippe B, Richter J M, Alsari M, Booker E P, Hutter E M, Pearson A J, Lilliu S, Savenije T J, Rensmo H, Divitini G, Ducati C, Friend R H and Stranks S D 2018 *Nature* **555** 497
[8] Bi D, Yi C, Luo J, Décoppet J D, Zhang F, Zakeeruddin Shaik M, Li X, Hagfeldt A and Grätzel M 2016 *Nat. Energy* **1** 16142
[9] Dai Q, Luo C, Wang X, Gao F, Jiang X and Zhao Q 2022 *Chin. Phys. B* **31** 037303
[10] Jiang Q, Zhao Y, Zhang X, Yang X, Chen Y, Chu Z, Ye Q, Li X, Yin Z and You J 2019 *Nat. Photon.* **13** 460
[11] Ke W, Fang G, Wan J, Tao H, Liu Q, Xiong L, Qin P, Wang J, Lei H, Yang G, Qin M, Zhao X and Yan Y 2015 *Nat. Commun.* **6** 6700
[12] Kojima A, Teshima K, Shirai Y and Miyasaka T 2009 *Journal of the American Chemical Society* **131** 6050
[13] Lee M M, Teuscher J, Miyasaka T, Murakami T N and Snaith H J 2012 *Science* **338** 643
[14] Min H, Lee D Y, Kim J, Kim G, Lee K S, Kim J, Paik M J, Kim Y K, Kim K S, Kim M G, Shin T J and Il Seok S 2021 *Nature* **598** 444
[15] Qu Z, Ma F, Zhao Y, Chu X, Yu S and You J 2021 *Chin. Phys. Lett.* **38** 107801
[16] Tan H, Jain A, Voznyy O, Lan X, Arquer F P G D, Fan J Z, Quintero-Bermudez R, Yuan M, Zhang B, Zhao Y, Fan F, Li P, Quan L N, Zhao Y, Lu Z H, Yang Z, Hoogland S and Sargent E H 2017 *Science* **355** 722
[17] Yu Zhan W C, Fu Yang and Li Y 2021 *Chin. Phys. B* **30** 88803
[18] Zheng X, Chen B, Dai J, Fang Y, Bai Y, Lin Y, Wei H, Zeng Xiao C and Huang J 2017 *Nat. Energy* **2** 17102
[19] https://www.nrel.gov/pv/assets/pdfs/best-research-cell-efficiencies-rev220126.pdf
[20] Baikie T, Fang Y, Kadro J M, Schreyer M, Wei F, Mhaisalkar S G, Graetzel M and White T J 2013 *Journal of Materials Chemistry A* **1** 5628
[21] Berhe T A, Su W N, Chen C H, Pan C J, Cheng J H, Chen H M, Tsai M C, Chen L Y, Dubale A A and Hwang B J 2016 *Energy & Environmental Science* **9** 323
[22] Saparov B and Mitzi D B 2016 *Chemical Reviews* **116** 4558
[23] Stranks S D and Snaith H J 2015 *Nat. Nanotech.* **10** 391
[24] Djurišić A B, Liu F Z, Tam H W, Wong M K, Ng A, Surya C, Chen W and He Z B 2017 *Progress in Quantum Electronics* **53** 1
[25] Park J H, Seo J, Park S, Shin S S, Kim Y C, Jeon N J, Shin H W, Ahn T K, Noh J H, Yoon S C, Hwang C S and Seok S I 2015 *Adv. Mater.* **27** 4013
[26] Jeng J Y, Chiang Y F, Lee M H, Peng S R, Guo T F, Chen P and Wen T C 2013 *Adv. Mater.* **25** 3727
[27] Li Z, Li B, Wu X, Sheppard S A, Zhang S, Gao D, Long N J and Zhu Z 2022 *Science* **376** 416
[28] Liu T, Chen K, Hu Q, Zhu R and Gong Q 2016 *Advanced Energy Materials* **6** 1600457
[29] Yang X, Luo D, Xiang Y, Zhao L, Anaya M, Shen Y, Wu J, Yang W, Chiang Y H, Tu Y, Su R, Hu Q, Yu H, Shao G, Huang W, Russell T P, Gong Q, Stranks S D, Zhang W and Zhu R 2021 *Adv. Mater.* **33** 2006435
[30] Bagheri Z, Matteocci F, Lamanna E, Di Girolamo D, Marrani A G, Zanoni R, Di Carlo A and Moshaii A 2020 *Solar Energy Materials and Solar Cells* **215** 110606
[31] Luo D, Yang W, Wang Z, Sadhanala A, Hu Q, Su R, Shivanna R, Trindade G F, Watts J F, Xu Z, Liu T, Chen K, Ye F, Wu P, Zhao L, Wu J, Tu Y, Zhang Y, Yang X, Zhang W, Friend R H, Gong Q, Snaith H J and Zhu R 2018 *Science* **360** 1442
[32] Wang H, Song Y, Kang Y, Dang S, Feng J and Dong Q 2020 *Journal of Materials Chemistry A* **8** 7309
[33] Li X, Zhang W, Guo X, Lu C, Wei J and Fang J 2022 *Science* **375** 434
[34] Degani M, An Q, Albaladejo-Siguan M, Hofstetter Y J, Cho C, Paulus F, Grancini G and Vaynzof Y 2021 *Science Advances* **7** eabj7930
[35] Zhou Q, Qiu J, Wang Y, Yu M, Liu J and Zhang X 2021 *ACS Energy Letters* **6** 1596
[36] Chen S, Dai X, Xu S, Jiao H, Zhao L and Huang J 2021 *Science* **373** 902
[37] Wu S, Zhang J, Li Z, Liu D, Qin M, Cheung S H, Lu X, Lei D, So S K, Zhu Z and Jen A K Y 2020 *Joule* **4** 1248
[38] Li X, Liu X, Wang X, Zhao L, Jiu T and Fang J 2015 *Journal of Materials Chemistry A* **3** 15024
[39] Li X, Wang Y C, Zhu L, Zhang W, Wang H Q and Fang J 2017 *ACS Applied Materials & Interfaces* **9** 31357
[40] Li J, Zhao M, Zhao C, Jian H, Wang N, Yao L, Huang C, Zhao Y and Jiu T 2019 *ACS Applied Materials & Interfaces* **11** 2626
[41] Li S, He B, Xu J, Lu H, Jiang J, Zhu J, Kan Z, Zhu L and Wu F 2020 *Nanoscale* **12** 3686
[42] Li X, Zhang W, Guo X, Lu C, Wei J and Fang J 2022 *Science* **375** 434

[43] Kim S Y, Cho S J, Byeon S E, He X and Yoon H J 2020 *Advanced Energy Materials* **10** 2002606
[44] Magomedov A, Al-Ashouri A, Kasparavičius E, Strazdaite S, Niaura G, Jošt M, Malinauskas T, Albrecht S and Getautis V 2018 *Advanced Energy Materials* **8** 1801892
[45] Metoki N, Liu L, Beilis E, Eliaz N and Mandler D 2014 *Langmuir* **30** 6791
[46] Azmi R, Ugur E, Seitkhan A, Aljamaan F, Subbiah A S, Liu J, Harrison G T, Nugraha M I, Eswaran M K, Babics M, Chen Y, Xu F, Allen T G, Rehman A U, Wang C L, Anthopoulos T D, Schwingenschlogl U, De Bastiani M, Aydin E and De Wolf S 2022 *Science* **376** 73
[47] Al-Ashouri A, Kohnen E, Li B, *et al.* 2020 *Science* **370** 1300
[48] Al-Ashouri A, Magomedov A, Ross M, *et al.* 2019 *Energy & Environmental Science* **12** 3356
[49] Gharibzadeh S, Fassl P, Hossain I M, Rohrbeck P, Frericks M, Schmidt M, Duong T, Khan M R, Abzieher T, Nejand B A, Schackmar F, Almora O, Feeney T, Singh R, Fuchs D, Lemmer U, Hofmann J P, Weber S a L and Paetzold U W 2021 *Energy & Environmental Science* **14** 5875
[50] Levine I, Al-Ashouri A, Musiienko A, Hempel H, Magomedov A, Drevilkauskaite A, Getautis V, Menzel D, Hinrichs K, Unold T, Albrecht S and Dittrich T 2021 *Joule* **5** 2915
[51] Aktas E, Phung N, Köbler H, González D A, Méndez M, Kafedjiska I, Turren-Cruz S H, Wenisch R, Lauermann I, Abate A and Palomares E 2021 *Energy & Environmental Science* **14** 3976
[52] Liao Q, Wang Y, Zhang Z, Yang K, Shi Y, Feng K, Li B, Huang J, Gao P and Guo X 2022 *Journal of Energy Chemistry* **68** 87
[53] Ullah A, Park K H, Nguyen H D, Siddique Y, Shah S F A, Tran H, Park S, Lee S I, Lee K K, Han C H, Kim K, Ahn S, Jeong I, Park Y S and Hong S 2022 *Advanced Energy Materials* **12** 2103175
[54] Li L, Gibson E A, Qin P, Boschloo G, Gorlov M, Hagfeldt A and Sun L 2010 *Advanced Materials* **22** 1759
[55] Manders J R, Tsang S W, Hartel M J, Lai T H, Chen S, Amb C M, Reynolds J R and So F 2013 *Advanced Functional Materials* **23** 2993
[56] Liu S, Liu R, Chen Y, Ho S, Kim J H and So F 2014 *Chemistry of Materials* **26** 4528
[57] Arumugam G M, Karunakaran S K, Liu C, Zhang C, Guo F, Wu S and Mai Y 2021 *Nano Select* **2** 1081
[58] Docampo P, Ball J M, Darwich M, Eperon G E and Snaith H J 2013 *Nat. Commun.* **4** 2761
[59] Wang T, Ding D, Zheng H, Wang X, Wang J, Liu H and Shen W 2019 *Solar RRL* **3** 1900045
[60] Seo S, Park I J, Kim M, Lee S, Bae C, Jung H S, Park N G, Kim J Y and Shin H 2016 *Nanoscale* **8** 11403
[61] Koushik D, Jošt M, Dučinskas A, Burgess C, Zardetto V, Weijtens C, Verheijen M A, Kessels W M M, Albrecht S and Creatore M 2019 *Journal of Materials Chemistry C* **7** 12532
[62] Bai Y, Chen H, Xiao S, Xue Q, Zhang T, Zhu Z, Li Q, Hu C, Yang Y, Hu Z, Huang F, Wong K S, Yip H L and Yang S 2016 *Advanced Functional Materials* **26** 2950
[63] Wang Q, Chueh C C, Zhao T, Cheng J, Eslamian M, Choy W C H and Jen A K Y 2017 *ChemSusChem* **10** 3794
[64] Phung N, Verheijen M, Todinova A, Datta K, Verhage M, Al-Ashouri A, Köbler H, Li X, Abate A, Albrecht S and Creatore M 2022 *ACS Applied Materials & Interfaces* **14** 2166
[65] Li Z, Jo B H, Hwang S J, Kim T H, Somasundaram S, Kamaraj E, Bang J, Ahn T K, Park S and Park H J 2019 *Advanced Science* **6** 1802163
[66] Lian X, Chen J, Shan S, Wu G and Chen H 2020 *ACS Applied Materials & Interfaces* **12** 46340
[67] Wang Y, Ju H, Mahmoudi T, Liu C, Zhang C, Wu S, Yang Y, Wang Z, Hu J, Cao Y, Guo F, Hahn Y B and Mai Y 2021 *Nano Energy* **88** 106285
[68] Jung J W, Chueh C C and Jen A K Y 2015 *Adv. Mater.* **27** 7874
[69] Yao K, Li F, He Q, Wang X, Jiang Y, Huang H and Jen A K Y 2017 *Nano Energy* **40** 155
[70] Feng M, Wang M, Zhou H, Li W, Wang S, Zang Z and Chen S 2020 *ACS Applied Materials & Interfaces* **12** 50684
[71] Chen W, Zhou Y, Chen G, Wu Y, Tu B, Liu F Z, Huang L, Ng A M C, Djurišić A B and He Z 2019 *Advanced Energy Materials* **9** 1803872
[72] Xu J, Buin A, Ip A H, Li W, Voznyy O, Comin R, Yuan M, Jeon S, Ning Z, Mcdowell J J, Kanjanaboos P, Sun J P, Lan X, Quan L N, Kim D H, Hill I G, Maksymovych P and Sargent E H 2015 *Nat. Commun.* **6** 7081
[73] Sun X, Ji L Y, Chen W W, Guo X, Wang H H, Lei M, Wang Q and Li Y F 2017 *Journal of Materials Chemistry A* **5** 20720
[74] Shao Y, Xiao Z, Bi C, Yuan Y and Huang J 2014 *Nat. Commun.* **5** 5784
[75] Chen C, Zhang S, Wu S, Zhang W, Zhu H, Xiong Z, Zhang Y and Chen W 2017 *RSC Advances* **7** 35819
[76] Li D, Kong W, Zhang H, Wang D, Li W, Liu C, Chen H, Song W, Gao F, Amini A, Xu B, Li S and Cheng C 2020 *ACS Applied Materials & Interfaces* **12** 20103
[77] Chueh C C, Li C Z, Ding F, Li Z A, Cernetic N, Li X and Jen A K Y 2017 *ACS Applied Materials & Interfaces* **9** 1136
[78] Yang D, Zhang X, Wang K, Wu C, Yang R, Hou Y, Jiang Y, Liu S and Priya S 2019 *Nano Lett.* **19** 3313
[79] Wang J and Zhan X 2021 *Accounts of Chemical Research* **54** 132
[80] Wang S, Chen H, Zhang J, Xu G, Chen W, Xue R, Zhang M, Li Y and Li Y 2019 *Adv. Mater.* **31** 1903691
[81] Jiang Y, Wang J, Zai H, Ni D, Wang J, Xue P, Li N, Jia B, Lu H, Zhang Y, Wang F, Guo Z, Bi Z, Xie H, Wang Q, Ma W, Tu Y, Zhou H and Zhan X 2022 *Journal of the American Chemical Society* **144** 5400
[82] Mann D S, Patil P, Kim D H, Kwon S N and Na S I 2020 *Journal of Power Sources* **477** 228738
[83] Troughton J, Neophytou M, Gasparini N, Seitkhan A, Isikgor F H, Song X, Lin Y H, Liu T, Faber H, Yengel E, Kosco J, Oszajca M F, Hartmeier B, Rossier M, Lüchinger N A, Tsetseris L, Snaith H J, De Wolf S, Anthopoulos T D, Mcculloch I and Baran D 2020 *Energy & Environmental Science* **13** 268
[84] Hu X, Liu C, Zhang Z, Jiang X F, Garcia J, Sheehan C, Shui L, Priya S, Zhou G, Zhang S and Wang K 2020 *Advanced Science* **7** 2001285
[85] Brinkmann K O, Zhao J, Pourdavoud N, Becker T, Hu T, Olthof S, Meerholz K, Hoffmann L, Gahlmann T, Heiderhoff R, Oszajca M F, Luechinger N A, Rogalla D, Chen Y, Cheng B and Riedl T 2017 *Nat. Commun.* **8** 13938
[86] Chen H, Teale S, Chen B, Hou Y, Grater L, Zhu T, Bertens K, Park S M, Atapattu H R, Gao Y, Wei M, Johnston A K, Zhou Q, Xu K, Yu D, Han C, Cui T, Jung E H, Zhou C, Zhou W, Proppe A H, Hoogland S, Laquai F, Filleter T, Graham K R, Ning Z and Sargent E H 2022 *Nat. Photon.* **16** 352
[87] Lin R, Xu J, Wei M, Wang Y, Qin Z, Liu Z, Wu J, Xiao K, Chen B, Park S M, Chen G, Atapattu H R, Graham K R, Xu J, Zhu J, Li L, Zhang C, Sargent E H and Tan H 2022 *Nature* **603** 73
[88] Yu Z, Yang Z, Ni Z, Shao Y, Chen B, Lin Y, Wei H, Yu Z J, Holman Z and Huang J 2020 *Nat. Energy* **5** 657
[89] Lin Y H, Sakai N, Da P, Wu J, Sansom H C, Ramadan A J, Mahesh S, Liu J, Oliver R D J, Lim J, Aspitarte L, Sharma K, Madhu P K, Morales-Vilches A B, Nayak P K, Bai S, Gao F, Grovenor C R M, Johnston M B, Labram J G, Durrant J R, Ball J M, Wenger B, Stannowski B and Snaith H J 2020 *Science* **369** 96
[90] Bai S, Da P, Li C, Wang Z, Yuan Z, Fu F, Kawecki M, Liu X, Sakai N, Wang J T W, Huettner S, Buecheler S, Fahlman M, Gao F and Snaith H J 2019 *Nature* **571** 245
[91] Li D, Huang Y, Wang G, Lian Q, Shi R, Zhang L, Wang X, Gao F, Kong W, Xu B, Cheng C and Li S 2021 *Journal of Materials Chemistry A* **9** 12746
[92] Caprioglio P, Cruz D S, Caicedo-Dávila S, Zu F, Sutanto A A, Peña-Camargo F, Kegelmann L, Meggiolaro D, Gregori L, Wolff C M, Stiller B, Perdigón-Toro L, Köbler H, Li B, Gutierrez-Partida E, Lauermann I, Abate A, Koch N, De Angelis F, Rech B, Grancini G, Abou-Ras D, Nazeeruddin M K, Stolterfoht M, Albrecht S, Antonietti M and Neher D 2021 *Energy & Environmental Science* **14** 4508
[93] Yang S, Dai J, Yu Z, Shao Y, Zhou Y, Xiao X, Zeng X C and Huang J 2019 *Journal of the American Chemical Society* **141** 5781
[94] Wu W Q, Rudd P N, Wang Q, Yang Z and Huang J 2020 *Adv. Mater.* **32** 2000995
[95] Li F, Deng X, Qi F, Li Z, Liu D, Shen D, Qin M, Wu S, Lin F, Jang S H, Zhang J, Lu X, Lei D, Lee C S, Zhu Z and Jen A K Y 2020 *Journal of the American Chemical Society* **142** 20134
[96] Zhang F, Ye S, Zhang H, Zhou F, Hao Y, Cai H, Song J and Qu J 2021 *Nano Energy* **89** 106370
[97] Tan S, Huang T, Yavuz I, Wang R, Yoon T W, Xu M, Xing Q, Park K, Lee D K, Chen C H, Zheng R, Yoon T, Zhao Y, Wang H C, Meng D, Xue J, Song Y J, Pan X, Park N G, Lee J W and Yang Y 2022 *Nature* **605** 268